Asian Journal of Engineering and Technology (ISSN: 2321 – 2462)
Volume 03 – Issue 05, October 2015

Temperature Impact in Electromagnetic Non-Invasive Water/Oil/Gas Multiphase Real Time Monitoring

Samheri Almuradi[1*], Adnan A.Abdul Rasool[2], Dhirgham Alkafaji[3], Muhammad Ateeq[4], Ahmed Al-shamma'a[5]

[1L]lecturer, Al-mustansiriya University, College of Engineering, Mech. Eng. Dept., Baghdad, Iraq,

[2] Assistant Professor, Al-mustansiriya University, College of Engineering, Mech. Eng. Dept., Baghdad, Iraq

[3] Assistant Professor, Babylon University, College of Engineering, Mech. Eng. Dept. Babylon, Iraq

[4] Research Assistant, Radio Frequency & Microwave Group, Faculty of Technology and Environment, Liverpool John Moores University, Liverpool, UK.

[5] Dean, Professor, Faculty of Technology and Environment, Liverpool John Moores University, Liverpool, UK.

[*]*Corresponding author's email: samheri_a [AT] yahoo.com*

ABSTRACT— ***The measurement of the reflected S-parameter (S_{11}) for multiphase (liquid-liquid-gas) 10-60% water, 70-20% oil and 20% gas (air) in volume are monitored using an electromagnetic microwave resonation method at a frequency range of 1-6 GHz. The measurements were examined at variable temperature ranges from 5-60 ^oC that were stepped by 5 ^oC. Clear shifts are observed in three resonant peaks of the S-parameter measurements as a volume fraction of mixture constituents. These are changed by 10% per step. The two frequency type (horizontal) S_{11} shifts take place at main (4 GHz frequency) and around 5 GHz frequency resonant peaks and one power type (vertical) shift at 5.45 GHz frequency resonant peak. When the temperature is held constant, the S_{11} values for all resonant peaks increase as WVF (water volume fraction) in the mixture increases. When WVF is held constant, the values of S_{11} increase as the temperature increases for around 5 GHz, 5.45 GHz frequency peaks and decreases for main peak. The results are validated by HFSS simulation executed for all tested volume fractions at 5 and 60 ^oC. For verification, a complete simulation is carried out at 40-40-20 percent of water-oil-gas and compared with experimental results at 5 ^oC intervals from 5-60 ^oC. The experimental results agreed well with theoretical predictions that simulated the HFSS software package with a maximum error of 1.91% for 5 ^oC mixtures and 1.13% for 60 ^oC mixtures at the main peak and 5.4% for 5 ^oC mixtures and 6.01% for 60 ^oC mixtures at 5.45 GHz peak. The study shows that the S_{11} measurements can be used as a dependent method to specify both the phase fraction of the multiphase mixture as well as its salinity and temperature.***

Keywords— Non-invasive, Electromagnetic, Water-Oil-Gas Multiphase, Temperature

1. INTRODUCTION

The huge advances in extracting and producing oil tools at different circumferences have led to the use of electromagnetic devices in multiphase monitoring. This development attracted wide attention in recent years. This monitoring was faced with complex flow patterns of multiphase water, oil and gas mixtures in addition to temperature impacts [1]. The effect of increasing the volume fraction of water in a multiphase water/oil/gas will affect the dielectric properties of the mixture. The environmental temperature differs as a function of location. The relative permittivity of water moves in an opposite direction of temperature, and the bulk conductivity has a direct relationship. As temperature increases, the strength and extent of the hydrogen bonding both decrease. This will:

(1) Lower both static and free surface permittivity,
(2) Lessen the difficulty for movement dipoles and allow the water molecule to oscillate at higher frequencies.
(3) Reduce the drag of water molecules and reduce friction and hence the dielectric loss.

(4) Increase the bulk conductivity of pure water from 0.0243 to 0.05 Siemens per meter corresponding to a temperature rise of 5 ^{o}C to 60 ^{o}C [2].

Much attention has been given to the use of microwaves (higher than 1 GHz frequency range) in electromagnetic techniques to find the volumetric phase fraction in recent years. This is because it is non-invasive, non-intrusive and offers real-time monitoring especially in oil production and extraction. It is an advanced oil instrument that can be used at different circumstances. The latest studies are limited to:

- Not more than two phase mixtures like liquid-liquid (water-oil) or liquid-gas (water or oil with gas).
- Lower frequency (radio) ranges with less sensitivity to resonance phenomena.
- Horizontal flow.
- Non-S-parameter (attenuation or phase) analysis methods that take a long time and much effort.
- Non-reflected (transmitted) S-parameter studies of higher power consumption.
- Non determining temperature.

S. Robinson and R. Nakkeeran (2012) [3] have designed an optical PC sensor to measure salinity at various temperatures. They employed the photonic crystal ring resonator to indicate and monitor the seawater salinity at 25 ^{o}C. The study showed an energy decrease at every 5% salinity increase step of seawater. The efficiency of the designed sensor is tested at variable temperatures. The study highlighted the dependency of such a sensor for real-time monitoring under different conditions. **A. Gryzlov et al. (2012) [4]** introduced a microwave sensor capable of measuring water conductivity in multiphase gas/liquid flows examined at different conditions. The sensor depended on a two-parameter measurement, and the differential attenuation and the differential phase, respectively. These—together with local information on the local flow regime—unambiguously measured the conductivity of the water phase. The test showed that the expected uncertainty of conductivity measurement was 0.5 S/m. The sensor has been tested within a conductivity range of 2-14 S/m through a test envelope that includes a gas volume fraction 0-90%, water-liquid ratios 60-100%, pressures of 5-125 bar and temperatures from 15 to 60 ^{o}C.
R. Lang et al. (2013) [5] used a capillary-tube with exit holes in a microwave resonating cavity at (L-band) at 1.415 GHz and 25-50 ^{o}C. This study showed an increase in both the relative permittivity and conductivity for all cases with and without a graphite cylinder. **Y. Li et al. (2013) [6]** studied the temperature and stress characteristics of a photonic band gap structure resonant cavities with square and graphite lattice using a finite–difference time domain method. The study showed more resonant frequency with cavity enlargement, and the curves between the resonant frequency and the temperature became a sectionalized line from a nonlinear curve. The temperature decreased as the cavity enlarged. This group showed that some structure in the center of the cavity will quickly increase the temperature sensitivity—this helped us design a temperature and stress sensor.
Yu.P. Filippov et al. (2014) [7] studied the effect of temperature in a model to describe a salty water in oil two phase mixture. They used a combination of a narrow device with a radio frequency sensor. They introduced the effect of temperature in an old salty water-oil model for higher accuracy. The modulated temperature shifted the resonant frequency. **El Abd (2014) [8]** compared two methods to measure the gas volume fraction of a two-phase mixture. The testing used scattering via gamma ray with transmission as well as traditional Compton and Compton-Compton methods. The results showed a higher accuracy via Compton-Compton scattering method than the others. The designed device was simple and much safer from radiation that could lead to a lower shielding. The device could be used for gamma ray demonstration. This method was suggested to be applied for other flow patterns in the future.
Zhao An et al. (2014) [9] measured a two phase hold-up of oil and water flowing horizontally. They used a sensor with concaved capacitor. They calculated the static response for different flow patterns and optimized the sensor. They conducted experiments to study the characteristics of the concave capacitance sensor. The sensor showed good performance for the dispersion of water in oil flow. The sensor has high sensitivity when the oil holdup is larger than 60%. The response of concaved capacitance sensor for six different oil-water flows of the two-phase horizontal model. Different patterns of flow were presented with mini conductance array probes, and the oil-holdup was obtained via quick closing of the valve. The measured results indicated that the optimized concave capacitance sensor has poor sensitivity for static and dynamic dispersions in water and oil in water but showed good performance for other flow patterns especially for dispersed static and dynamic water in oil with high oil holdup.
Chao Tan et al. (2014) [10] measured an oil-water two-phase flow using a conductance ring coupled cone CRCC meter. The CRCC meter utilized the spatial characteristics of the coupled cone and conductance rings to achieve more reliable estimates of flow rate and phase fraction. The sizes of the instruments were jointly optimized considering the overall pressure drop and sensitivity of electrical sensing field. The device was fabricated for static calibration and dynamic liquid-liquid (water and oil) mixture tests. The dynamic results showed that the proposed CRCC can deliver inferences on volume fraction of phase and individual flow rate with an associated average relative error below 5% after easy calibration. If a flow of two phase water and oil enters the annular channel, then phase occupation might have changed versus the full pipe cross-sectional-area. This may cause a change inversion point of phase, although the phase fraction remains the same. This further affects the measurement range of conductance rings. This was, however, a complicated

issue that needed further investigation and clarification. However, the proposed structure of CRCC provided a new way of integrating different measuring techniques for multiphase flow measurement because it improves the system for two phase liquid and gas mixtures.

S. Park et al. (2014) [11] measured complex permittivity and detected small permittivity changes as the temperature is slowly increased. This was done with simple technology—a partially open cavity. They worked at 1.2489375 to 1.2518125 GHz frequency and 25-60 ^{o}C. This method showed a better performance in measuring small dielectric constant changes than the open-ended probe. This agreed theoretically with the Cole-Cole equation. In the present study, the S-parameter shifting occurs in the single water liquid phase. It is compared with that of a multiphase mixture. Water is sensitive to dielectric substances in the multiphase (water-oil-gas). The scope of this study is to design and monitor the crude oil as a multiphase mixture of oil, water and gas extracted from oil wells. The ideal approach is real time, electromagnetic, accurate, non-invasive, unobtrusive, vertical flow direction, low power consumption and light weight. The approach should be simple and estimate both volume phase fraction and temperature of each oil, water and gas constituent.

2. THEORY

2.1 Relation between S-Parameter and Mixture Permittivity

The relation between the permittivity of the mixture and the measured reflected S-parameter (S_{11}) can be approximated as [12]:

$$S_{11} = \frac{\left(\frac{1}{R} - R\right)\left(e^{-\gamma d} - e^{-\gamma d}\right)}{D} \quad \ldots (1)$$

Here, R is the ratio of characteristic impedance with and without material under test, d is the diameter of material sample under test, D is the denominator quantity and γ is the propagation constant,

$$D = \left(R + \frac{1}{R} + 2\right)e^{\gamma d} - \left(R + \frac{1}{R} - 2\right)e^{-\gamma d} \quad \ldots (2)$$

$$R = \sqrt{\frac{1 - \left(\frac{f_c}{f}\right)^2}{\varepsilon'_{mr} - i\varepsilon''_{mr} - \left(\frac{f_c}{f}\right)^2}} \quad \ldots (3)$$

$$\gamma = i\frac{\omega}{C}\sqrt{\varepsilon'_{mr} - i\varepsilon''_{mr} - \left(\frac{f_c}{f}\right)^2} \quad \ldots (4)$$

Where f_c is the cut-off frequency.

2.2 Water Permittivity Analysis

Permittivity is a complex quantity used to describe the dielectric properties that influence reflection of EMW (electromagnetic waves) at interfaces and the attenuation of wave energy within materials [13]. The permittivity of a mixture material needs to know the permittivity of its constituents. The permittivity of water is:

$$\varepsilon_{r,w} = \varepsilon'_r - i\varepsilon''_r \quad \ldots (5)$$

The real part is referred to dielectric constant and represents the stored energy when the material is exposed to an electric field,

$$\varepsilon'_r = \frac{\varepsilon_s - \varepsilon_\infty}{1 + \omega^2\tau^2} + \varepsilon_\infty \quad \ldots (6)$$

Where ε_s and ε_∞ represent the static and infinite permittivity values and ω and τ represent angular frequency ($2\pi f$) in radians per second and relaxation time in seconds, respectively.

2.3 Temperature Impact

The temperature effect goes through finding the value of the relaxation time,

$$\tau = \frac{3\forall\vartheta}{k_b T} \quad \ldots (7)$$

Here, $\vartheta, T, \forall$ and k_b are the viscosity, absolute temperature, volume (equals $\frac{4}{3}\pi r^3$ for spherical molecules) and Boltzmann constant (1.3805E-23 J/K), respectively.

For non-spherical water molecules,

$$\tau = c_1\frac{\vartheta}{T} \quad \ldots (8)$$

and,

$$\vartheta = \vartheta_o e^{E_a/R_g T} \quad \ldots(9)$$

Here, s ϑ_o, E_a *and* R_g are reference temperature viscosity, activation energy and universal gas constant, respectively. $\varepsilon_s(T)$ in equation (7) can be approximated as [14, 15],

$$\varepsilon_s(T) = ae^{-bT} \quad \ldots(10)$$

where a=87.85306 and b=0.00456992.
The imaginary part is referred to as the dielectric loss factor and it is described as,

$$\varepsilon_r^{''} = \frac{(\varepsilon_s - \varepsilon_\infty)(\omega\tau)}{1+\omega^2\tau^2} + \frac{\sigma}{\omega\varepsilon_o} \quad \ldots(11)$$

where σ *and* ε_o are water ionic conductivity in Siemens/m and free space or vacuum permittivity (8.854E-12 F/m), respectively. The ionic conductivity shows an increase as temperature rises in the absence of salinity or impurities [16]. The permittivity of oil and gas can then be estimated. Even these values are far lower than for water, which are between 2.5-3.5 for oil and 1.0-1.5 for gas. Therefore, they have little effect on the value of mixture permittivity because water permittivity is about 80.

2.4 Relation between Power, Permittivity and Temperature

The relationship between temperature and electrical power at MWF can be approximated as [17]. Thus, we first rename the relative effective permittivity as a mixture permittivity as follows,

$$P = \omega\varepsilon_0\varepsilon_r^{''}E^2 = \rho C_p\frac{\Delta T}{\Delta t} \quad \ldots(12)$$

where C_p is the specific heat of water in $JKg^{-1}c^{o-1}$, ρ is the water density in Kgm^{-3}, Δt is the time duration in seconds, and E is the electrical field intensity in V/m according to plane electromagnetic wave propagation in a medium is described by

$$E = E_0 e^{-ikx} = E_0 e^{-ik'x}.e^{-ik''x} \quad \ldots(13)$$

where x is the propagation distance and k is the wave vector. The real part $k^{'}$ determines the phase of the wave, while the imaginary part $k^{''}$ determines the attenuation:

$$k^{'} = \frac{\omega}{c}\sqrt{\frac{\varepsilon_{mr}^{'}}{2}\left(1+\sqrt{1+\left(\frac{\varepsilon_{mr}^{''}}{\varepsilon_{mr}^{'}}\right)^2}\right)} \quad \ldots(14)$$

$$k^{''} = \frac{\omega}{c}\sqrt{\frac{\varepsilon_{mr}^{'}}{2}\left(-1+\sqrt{1+\left(\frac{\varepsilon_{mr}^{''}}{\varepsilon_{mr}^{'}}\right)^2}\right)} \quad \ldots(15)$$

Here, c is the light speed (3E+8 ms^{-1}). The subscript mr refers to the relative mixture. For the high loss situation,

$$\varepsilon_{mr}^{''} \gg \varepsilon_{mr}^{'} \quad \ldots(16)$$

$$k^{'} = k^{''} = k_o\sqrt{\frac{\varepsilon_{mr}^{''}}{2}} \quad \ldots(17)$$

where k_o is the wave vector in vacuum [1].

3. EXPERIMENTAL SET-UP

The experimental set-up consists of a resonator, which is a vertical aluminum cylinder cavity (sensor) especially designed at (LJMU) Liverpool John Moores University under expert laboratory staff as shown in Figure (1). The geometry inside the dimensions are 8.9 cm inside diameter and 9.8 cm height. The cavity contains three grooves—two are identical and present the excitation ports (P_1 and P_2) ($\emptyset = 3.14$ cm). They are located at a circular body circumference side central height. The first P_1 is an entrance for the transmitting antenna, while the second P_2 is for the receiving antenna. The antennae are mounted by a rectangular cover on the edges of the ports. The antennas are made of a loop circular copper metal type. The loop diameter is of 2.5 cm, and the wire diameter is 1.5 cm. They are positioned vertically inside the cavity. The upper groove ($\emptyset = 1.5$ cm) is an entrance of the static or dynamic testing sample tubes.

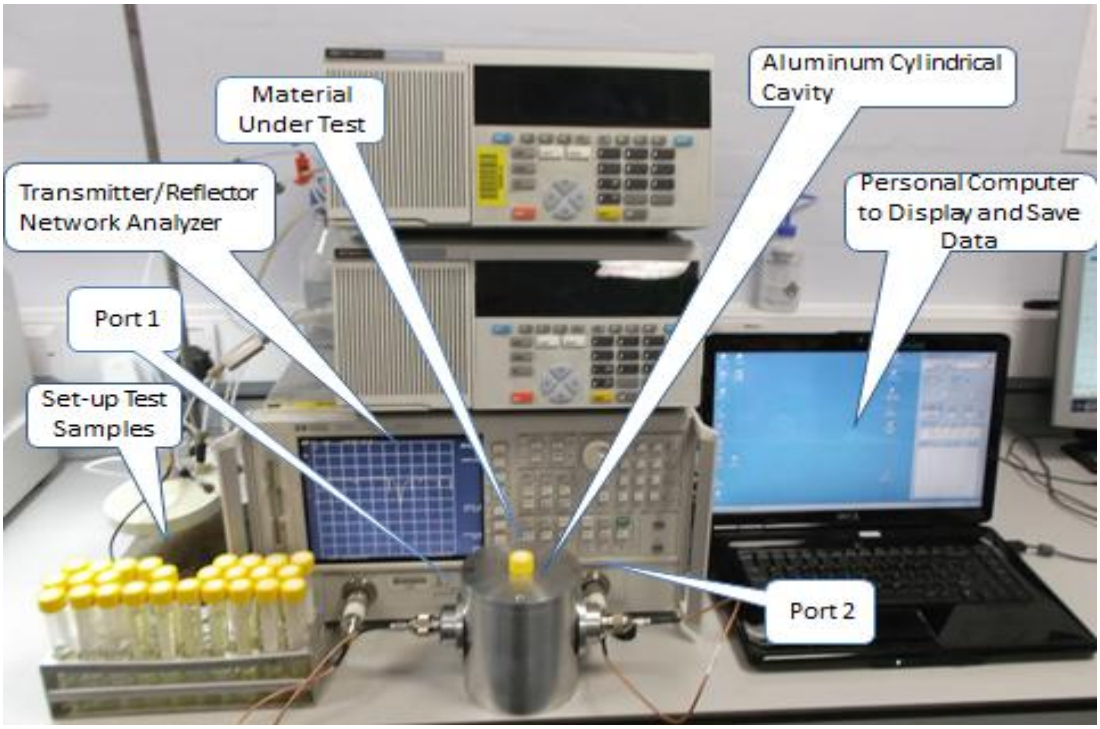

Figure 1: Experimental Set-up of Microwave Based Measurement System Using Cylindrical Cavity.

Sample tubes are made of polypropylene material 1 mm thick ($\varepsilon_r = 1.5$). Samples are preferably prepared according to volume fractions (water single phase and 60-10% multiphase, 20-70% oil and fixed fraction 20% gas (air) as shown in table (1).

Table 1: List of temperature samples prepared and tested in the microwave sensor.

Volume Fraction of Prepared Samples				
Sample #	**Water%**	**Oil%**	**Air%**	**Temperature (^{0}C)**
1	**100**	**0**	**0**	**5, 10, 15, 20, 25, 30, 35, 40, 45, 50, 55 and 60**
2	**10**	**70**	**20**	
3	**20**	**60**	**20**	
4	**30**	**50**	**20**	
5	**40**	**40**	**20**	
6	**50**	**30**	**20**	
7	**60**	**20**	**20**	

The samples are immersed in a variable temperature controlled pool to ensure that the inside multiphase substances are at 5-60 ^{o}C with 5 ^{o}C step sizes. Tested samples are equipped with long body temperature sensors that are used to fix the temperature of each sample within the required range see figure (2).

Figure 2: Samples Temperature Control.

The test results should be done at a certain time with a pre-fixed temperature. For governing the temperature, a temperature controlling method is used to fix the temperature in a certain limited range with very few allowed deviations. The difference between the readings before and after the test should be the same for all test samples. There is a heat transfer change with the surroundings as the multiphase test fractions change. A typical 2-port HP 8720 ET Transmission/Reflection vector network analyzer (VNA) is shown in figure (1). The analyzer is connected to P_1 and P_2 through precision cables and suitable connector adaptors. This type of VNA gives an accurate S11 measurement and is modified to work with the newest software data convertor. This can be saved and displayed directly on a personal computer easily and quickly. Prior to the VNA S-parameter measurements, the most important step is to perform an accurate calibration compatible with the present specified measurements. A full two port calibration was carried out to eliminate all sources of systematic errors. The calibration procedure worked from 1 to 6 GHz with typical selections of 1-801 points. The personal computer receives the data of S_{11} for the given frequency range. A real certainty is done before multiphase testing via single phase water, oil and gas sample measurements. This in turn is compared with the HFSS driven modal simulation according to the cavity geometry dimensions and actual affected properties and conditions of fixed and variable temperature range.

4. SIMULATION

EM simulation using Ansoft HFSS (High Frequency Structure Simulator) package version 13 is used to analyze the multiphase samples inside the cavity. Two solutions were studied. The first is the Eigen mode solver type to determine the resonant frequencies of the structure and the fields at those frequencies. Five modes were chosen at every minimum frequency 1-5 GHz with a maximum no. of 5 passes. The results were analyzed to find the resonant frequency at each minimum frequency chosen with their quality factors to specify the highest ones. This procedure was carried out for every single phase substance water, oil and gas (air) separately. Table (2) shows the results for these solutions.

The aim of the Eigen mode was to specify the range of working frequencies and solution frequencies at which the driven modal solution executed at the second stage of simulation. The driven modal was carried out in 10 passes and 0.01 maximum delta S-parameter at 3 GHz as the solution frequency. A frequency sweep discrete type from 1-6 GHz was set to 0.0062422 linear step size conditions. The effect of variable temperatures was modeled via input values of relative permittivity and bulk conductivity that correspond to 5-60 ^{o}C stepped by 5 ^{o}C for water according to Meissner and Wentz-Riseman and Wappling-Raaholt [17]. Oil, gas and other cavity materials were studied based on dielectric constants of various materials (Clipper Control, Inc.) [18]. The driven mode was done for all water volume fractions from 60-10%, 20-70% oil and 20% gas at different values of temperatures as mentioned before. To reduce the simulation run time for the mixtures, a symmetrical boundary is used for cylinder, ports and sample geometries by splitting them into one identical half.

Table 2: Resonant Frequencies for a Five Eigen Solution Analysis.

Frequency Range GHz	Water		Oil		Gas	
	Resonant Frequency GHz	Q-Factor	Resonant Frequency GHz	Q-Factor	Resonant Frequency GHz	Q-Factor
1-2	2.01468	268.704	3.54364	25597.8	1.53204	16476.8
2-3	2.10813	277.428	3.54118	25676.2	2.14735	28563.5
3-4	3.21270	427.932	4.40389	36908.3	3.02294	40560.6
4-5	4.16007	528.590	4.40308	36959.7	4.09199	43972.1
5-6	5.05525	2765.75	5.12781	41009.4	5.02243	68482.5

5. RESULTS AND DISCUSSION

Experimental or simulation S_{11} result figures show many peaks. Some of these peaks are resonance and others are not. The resonance peaks are peaks that change (resonance shift) when the sensor (resonator) acts via the material under test (multiphase mixture). Then, any change in the mixture constituent's volume percent or temperature will make a clear change in these peaks only. These peaks must be specified in advance as mentioned in the Eigen solution. They are part of the simulation procedure according to the same changes that are carried out in the experimental mixtures. Figure (3) shows the experimental variation of reflected S-parameter S_{11} for MW 1-6 GHz frequency spectrum of 100% single phase water only from 5-60 ^{o}C with temperature increments of 5 ^{o}C. The enlargement of frequency range between 3.5-4.5 GHz from the previous spectrum is shown in figure (4). A decrease in the S_{11} parameter (frequency horizontal shift) between 4.018199 to 4.011973 GHz according to the stepped temperature rise is obvious. Another enlargement in the frequency range between 4.5-6 GHz from the previous spectrum shows two shifts in figure (5). The power (vertical) shift at 5.45 GHz shows a frequency peak in which the S_{11} value increases from -4.59852 to -4.44581 dB as the temperature increases. A frequency (horizontal) shift occurs near the 5 GHz peak in which the S_{11} value increases from 5.20652 to 5.23913 GHz as the temperature increases. The relationship between S_{11} and temperature depends on the frequency values. It is governed by the equations mentioned above. Therefore it is reverse at ~4 GHz and becomes direct at ~5 GHz and higher.

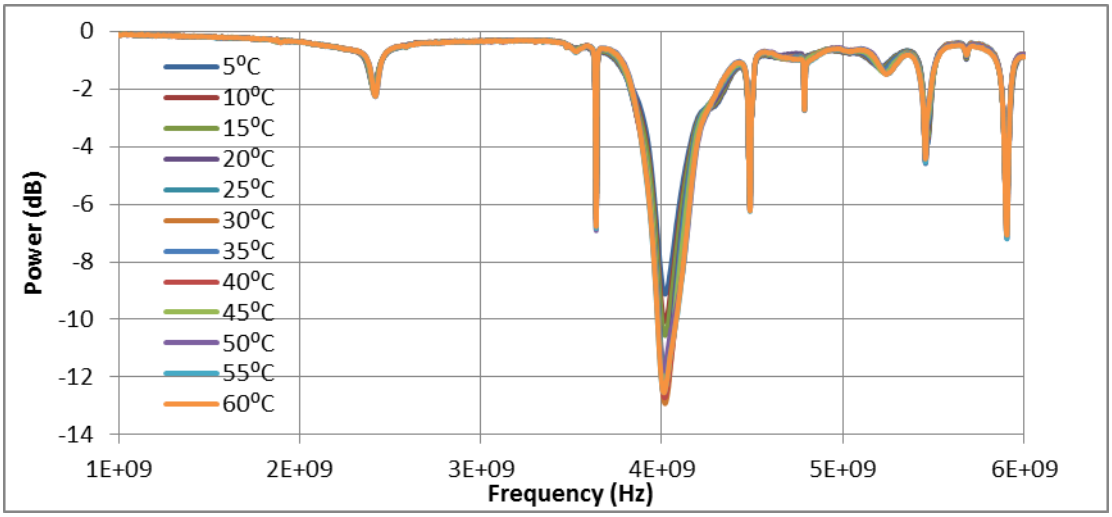

Figure 3: Experimental reflected S-parameter for different temperatures as a water single-phase at 1-6 GHz.

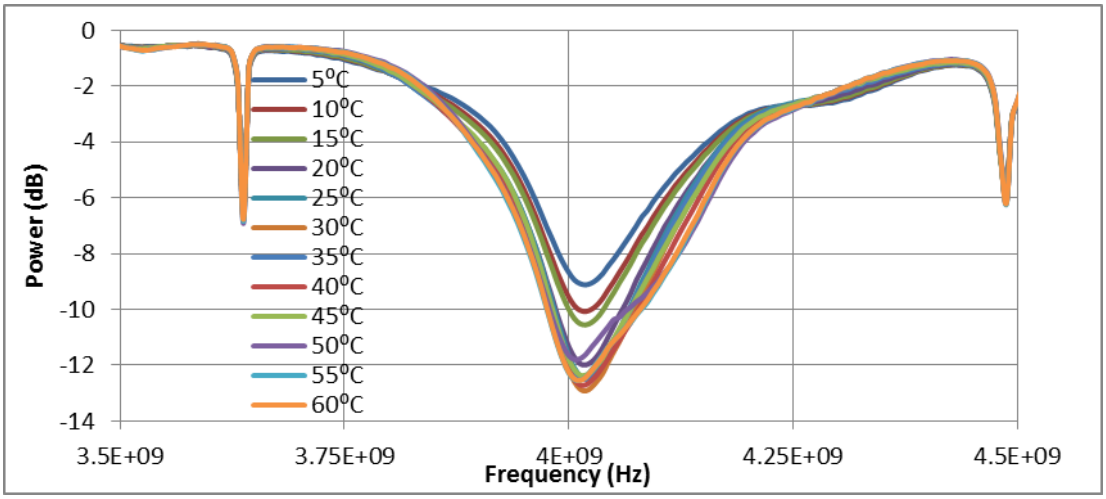

Figure 4: Experimental reflected S-parameter for different temperatures of the water single-phase at 3.5-4.5 GHz.

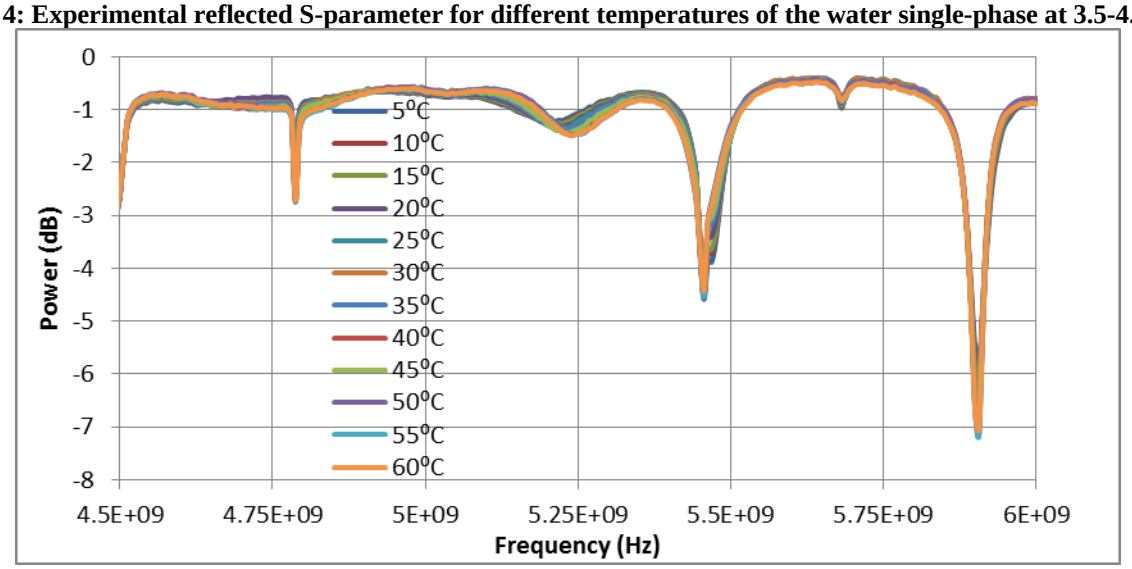

Figure 5: Experimental reflected S-parameter for different temperatures of water single-phase at 4.5-6 GHz.

Figure (6) shows the spectrum of frequency from 1-6 GHz. The experimental S_{11} with different tested temperature rises is shown for a three-phase mixture of 40% water, 40% oil and 20% gas.

Enlargements of the spectrum from 3.5-4.5 GHz and 4.5-6 GHz are presented in figures (7) and (8), respectively. The three shifts are clear. The temperature rises with the following distinct peaks:

- Main peak shift is from 4.00246 to 3.99016 GHz.
- Around 5 GHz, the peak shift is from 5.058 to 5.063 GHz.
- The 5.45 GHz peak shift is from -7.98 to -8.80 dB.

Table (3) summarizes the S_{11} measures of other volume fractions of the mixture.

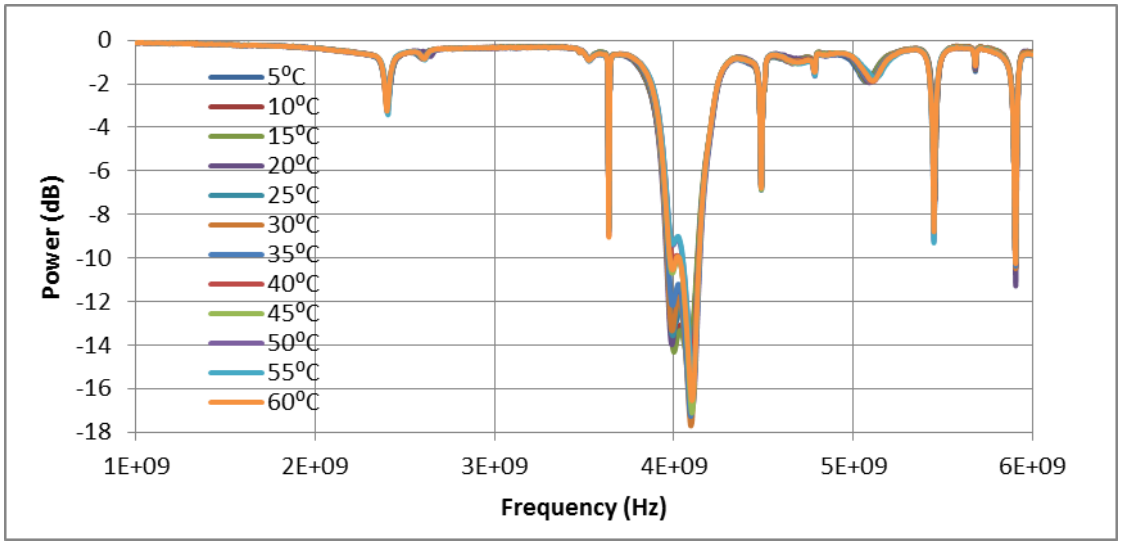

Figure 6: Experimental reflected S-parameter for different tested temperatures and 40% water, 40% oil and 20% gas three-phase at 1-6 GHz.

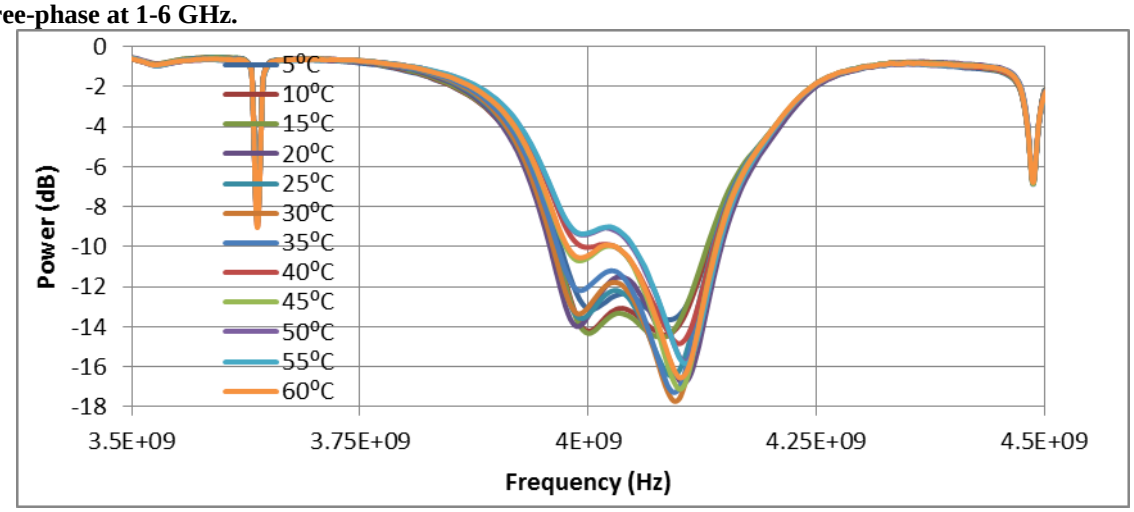

Figure 7: Experimental reflected S-parameter for different tested temperatures and 40% water, 40% oil and 20% gas three-phase at 3.5-4.5 GHz.

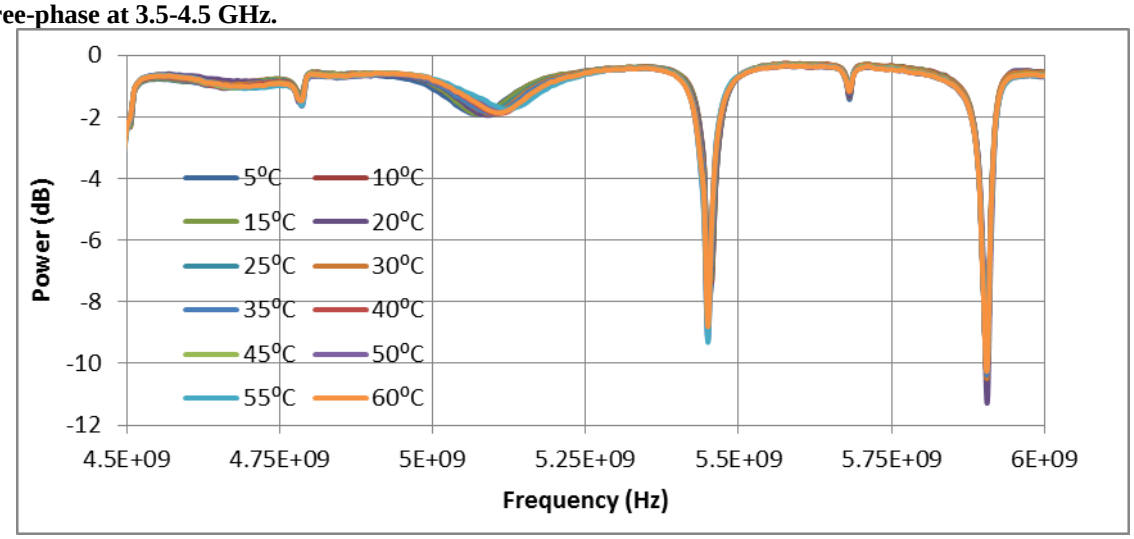

Figure 8: Experimental reflected S-parameter for different tested temperatures and 40% water, 40% oil and 20% gas three phase at 4.5-6 GHz.

Table 3: Experimental frequency and power S_{11} shifts with temperature variation at different water-oil-gas fractions.

Volume Fraction %			S_{11} Main Peak Frequency 1E09 Hz		S_{11} around 5 GHz Peak Frequency 1E09 Hz		S_{11} 5.45 GHz Peak Power dB	
Water%	Oil%	Gas%	5 °C	60 °C	5 °C	60 °C	5 °C	60 °C
10	70	20	3.95693	3.95545	4.950	4.950	-24.013	-19.431
20	60	20	3.96823	3.96584	4.955	4.953	-24.281	-20.034
30	50	20	3.98317	3.99837	5.058	5.063	-9.390	-13.905
40	40	20	4.00246	3.99016	5.071	5.108	-7.980	-8.800
50	30	20	4.01328	3.99526	5.079	5.125	-6.679	-5.424
60	20	20	4.01214	3.99757	5.085	5.129	-6.273	-5.073
100	0	0	4.01820	4.01197	5.207	5.239	-4.599	-4.446

Figure (9) shows the simulated S_{11} for different temperatures of 40% water, 40% oil and 20% gas three-phase mixture 1-6 GHz frequency spectrum. Figures (10) and (11) show the enlargements of 3.5-4.5 GHz and 4.5-6 GHz frequency ranges given in the previous figure.

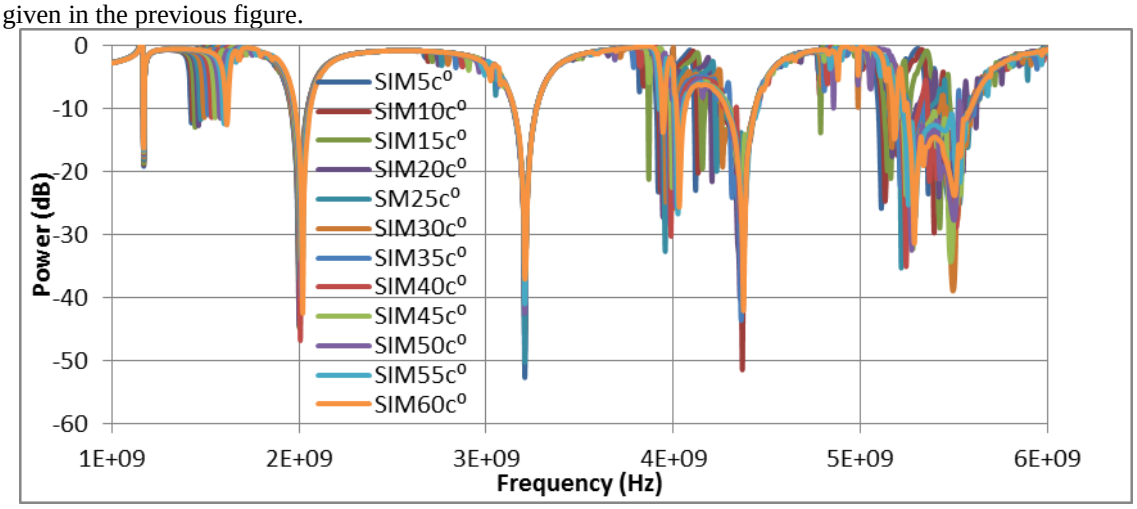

Figure 9: Simulated reflected S-parameter for different temperature samples of 40% water, 40% oil and 20% gas three phase at 1-6 GHz.

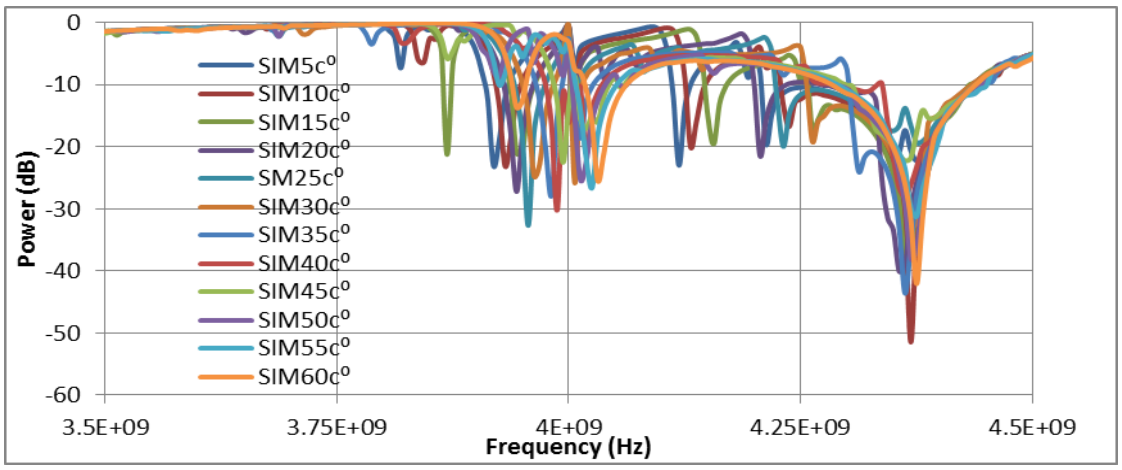

Figure 10: Simulated reflected S-parameter for different temperatures 40% water, 40% oil and 20% gas three phase at 3.5-4.5 GHz.

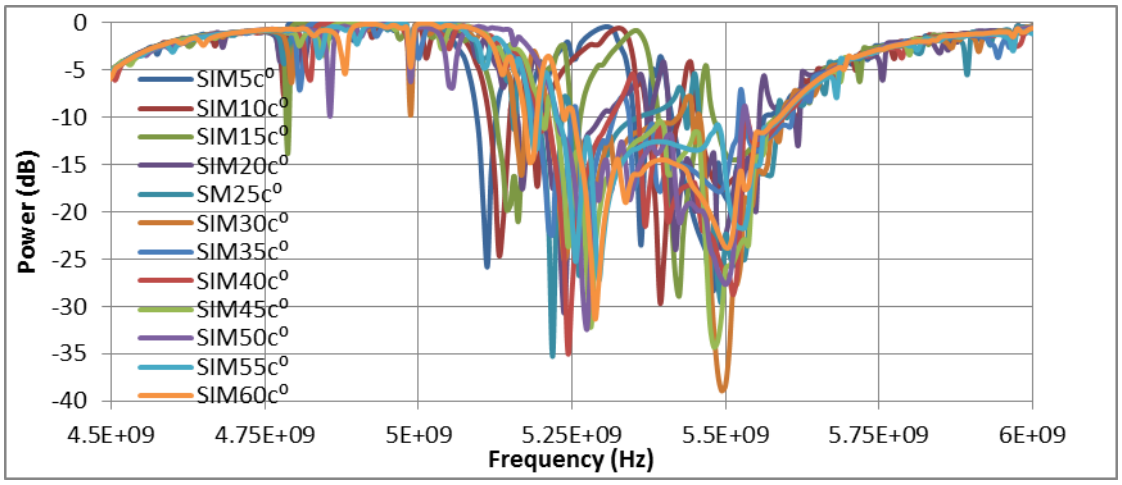

Figure 11: Simulated reflected S-parameter for different temperatures of 40% water, 40% oil and 20% gas three phase at 4.5-6 GHz.

The three figures above show a good agreement with experimental results—especially the three resonant peaks and their shifts as temperature change.

Figure (12) validates that the S_{11} shift in terms of experimental and simulated data at 5 ^{o}C from 10-60% WVF with 70-20% oil and fixed 20% gas. Figure (13) shows the S_{11} (main peak) shift S_{11} validation at 60 ^{o}C as volume fractions of mixture changes with 10% volume steps. These two figures present a good agreement between the experimental and simulated frequency shift results with maximum error of 1.91% for 5 ^{o}C mixtures and 1.13% for 60 ^{o}C mixtures.

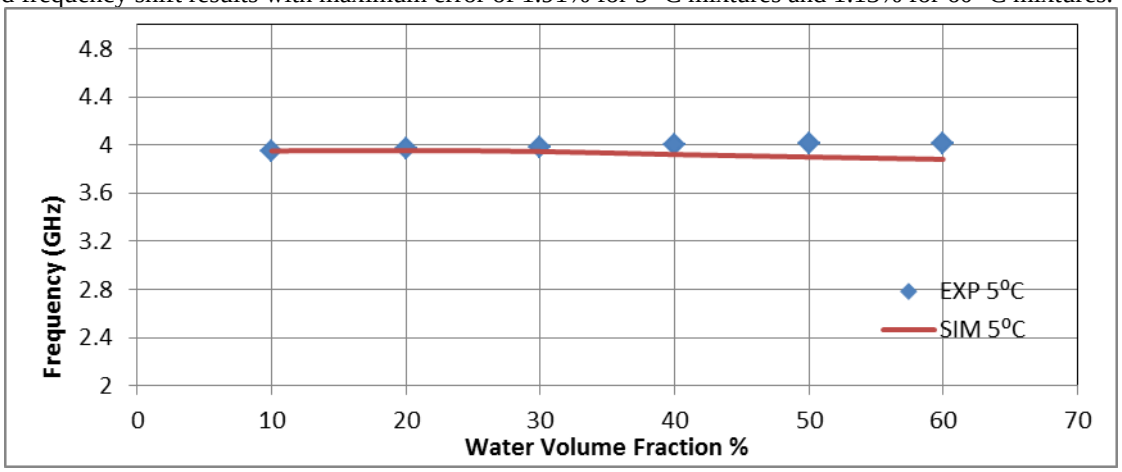

Figure 12: Frequency shift of experimental and simulated, reflected S-parameter validation (main peak) at 5 ^{o}C for (10-60%) water, (70-20%) oil and fixed 20% gas mixture.

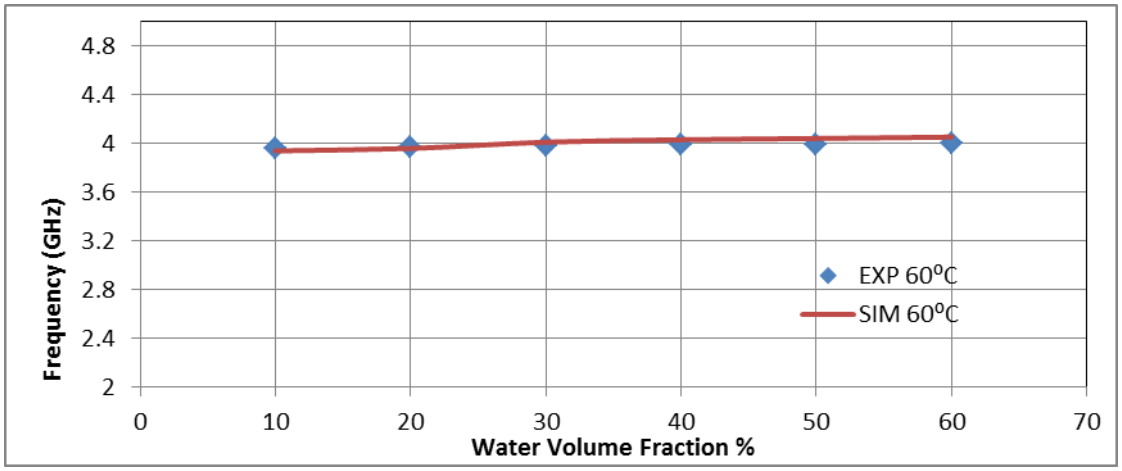

Figure 13: Frequency shift of experimental and simulated, reflected S-parameter validation (main peak) at 60 ^{o}C for (10-60%) water, (70-20%) oil and fixed 20% gas mixture.

Figures (14) and (15) show the S_{11} (around 5 GHz peak) shift of experimental and simulated validation at 5 ^{o}C and 60 ^{o}C, respectively, for 10-60% WVF, 70-20% oil and fixed 20% gas a three-phase mixture. The experimental and simulated agree well with a maximum error of 5.4% for 5 ^{o}C mixtures and 6.01% for 60 ^{o}C mixtures.

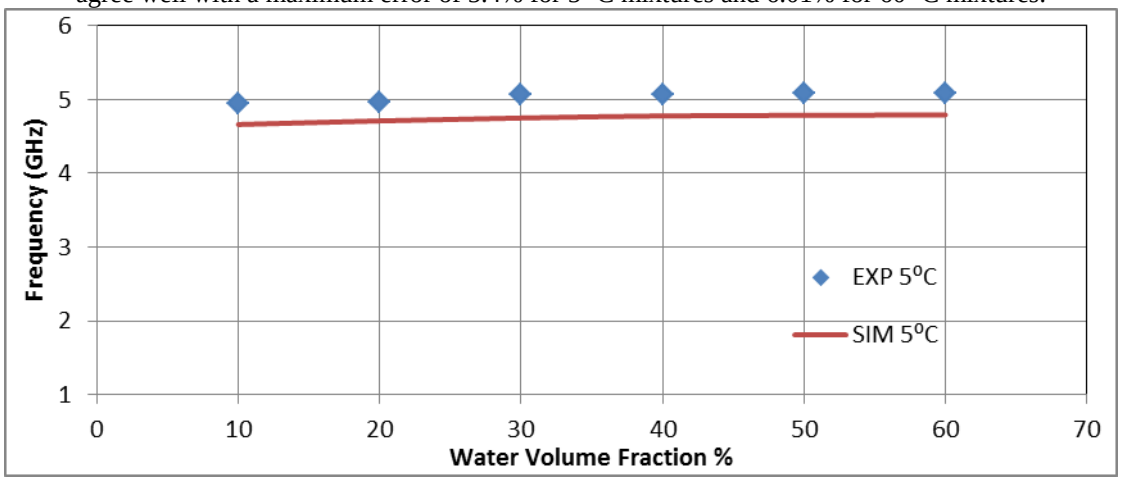

Figure 14: Frequency shift of experimental and simulated, reflected S-parameter validation (around 5 GHz) at 5 ^{o}C for (10-60%) water, (70-20%) oil and fixed 20% gas mixture.

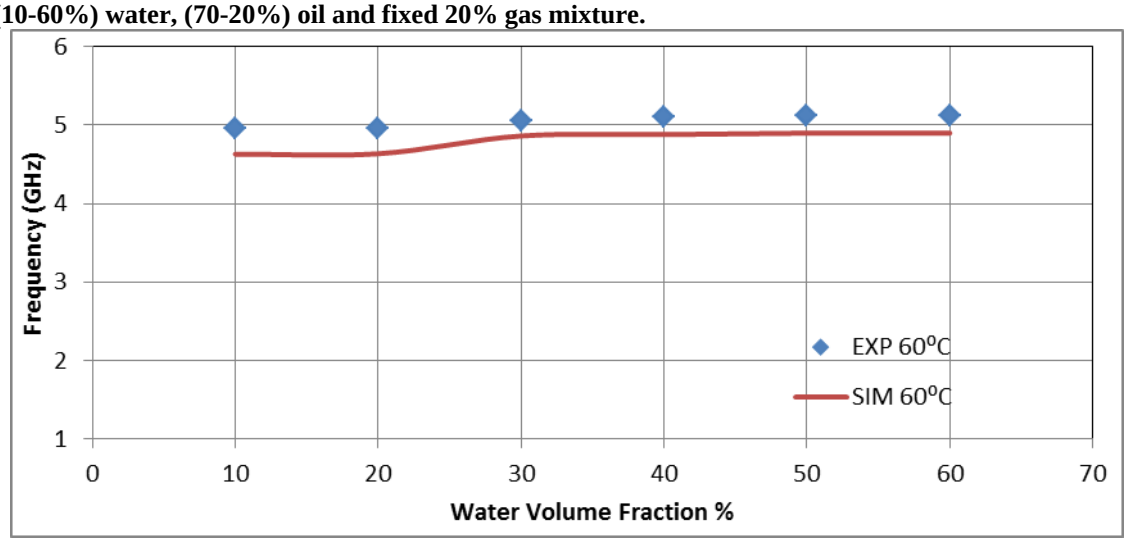

Figure 15: Frequency shift of experimental and simulated, reflected S-parameter validation (around 5 GHz) at 60 ^{o}C for (10-60%) water, (70-20%) oil and fixed 20% gas mixture.

The power shift for experimental and simulated S_{11} parameter validation of the 5.45 GHz peak is given in figures (16) and (17) for tested mixture temperatures of 5 ^{o}C and 60 ^{o}C respectively for a stepped 10-60% WVF, 70-20% oil and fixed 20% gas three phase. We see that the trend of the experimental and simulated results is identical. The jump in experimental values is attributed to the two sources of heat; the first comes from induced temperature changes and the other comes from microwave power. This is generated inside the cavity. This is the main reason that made a difference in temperature measurements before and after sample testing. This change is described well in equation (12). The second heat source must be added as ΔT to the simulation solver as an input overheat condition. This heat addition is noticed, and the temperature control measurement ensures this. The sample has a higher temperature after the test—this is true of tests at both lower and higher atmospheric temperatures.

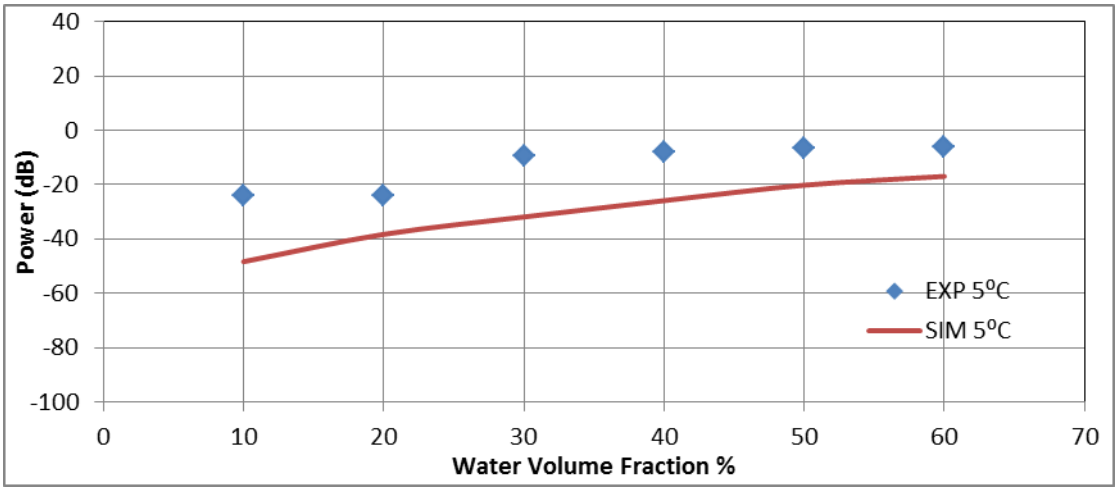

Figure 16: Power shift of experimental and simulated, reflected S-parameter validation (5.45 GHz frequency) at 5 °C for (10-60%) water, (70-20%) oil and fixed 20% gas mixture.

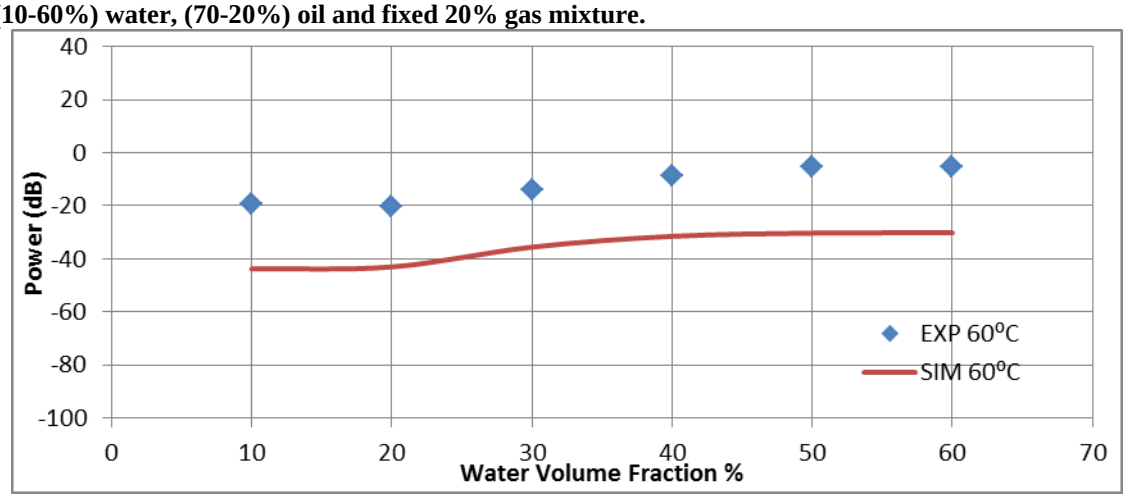

Figure 17: Power shift of experimental and simulated, reflected S-parameter validation (5.45 GHz frequency) at 60 °C for (10-60%) water, (70-20%) oil and fixed 20% gas mixture.

Figures (18) and (19) show the solved simulation mesh distribution in a cross-sectional area of cylindrical cavity at 5 °C and 60 °C multi-phase samples. In comparison, we can see that the critical mesh refinement is in the lower temperature regime.

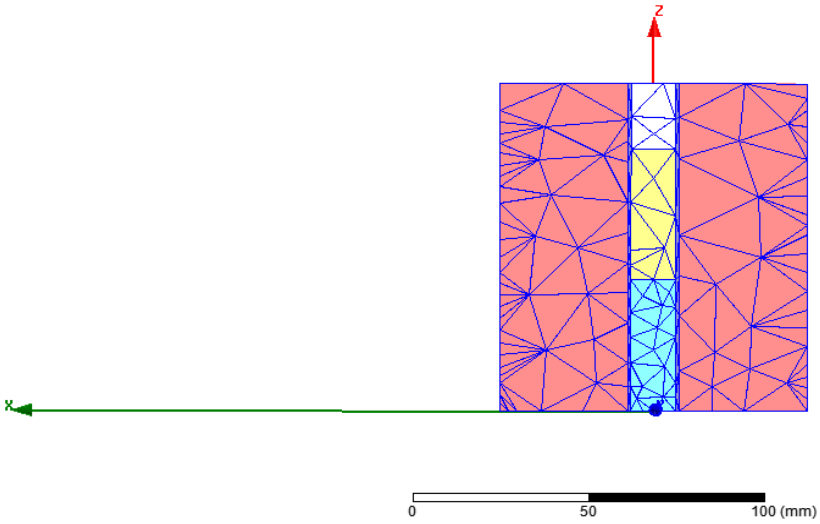

Figure 18: Vertical mesh distribution cross-section inside the cavity and sample for 5 °C of 40% water, 40% oil and 20% gas three-phase system.

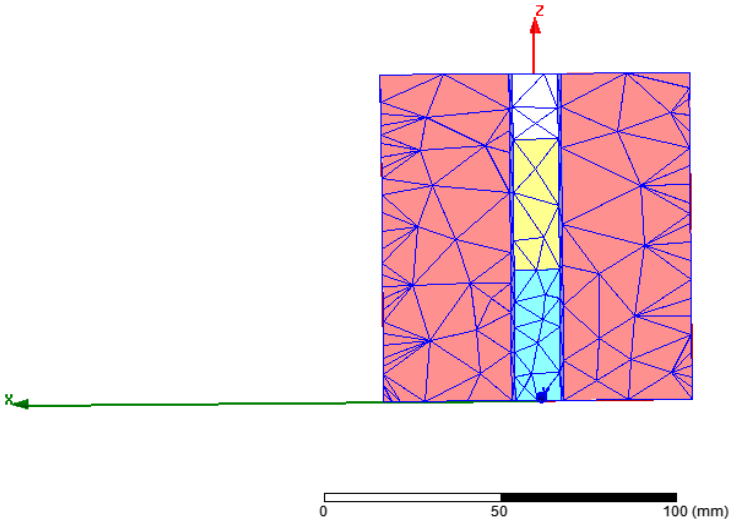

Figure 19: Vertical mesh distribution cross-section inside cavity and sample for 60 ^{o}C of 40% water, 40% oil and 20% gas three phase.

Figures (20) and (21) show the electrical field distribution in the cross-section of 5 ^{o}C and 60 ^{o}C samples. The 5 ^{o}C temperature multiphase sample shows an accumulation in EF (Electrical field) as opposed to the 60 ^{o}C sample.

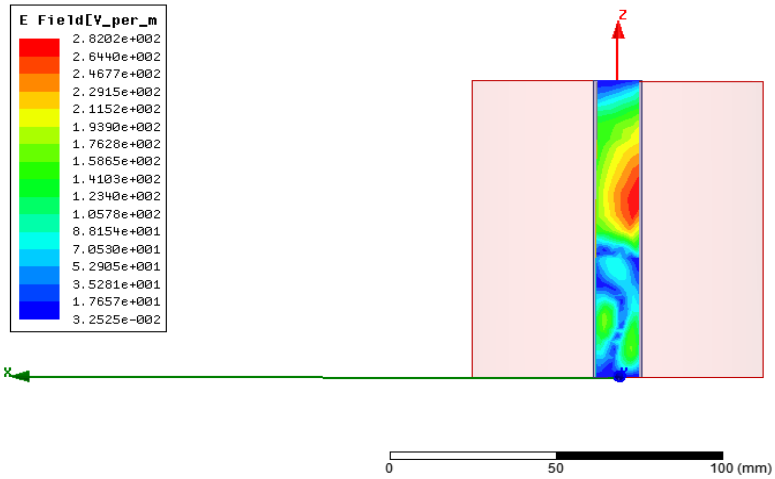

Figure 20: Vertical electrical field distribution cross-section inside sample for 5 ^{o}C of 40% water, 40% oil and 20% gas three phase.

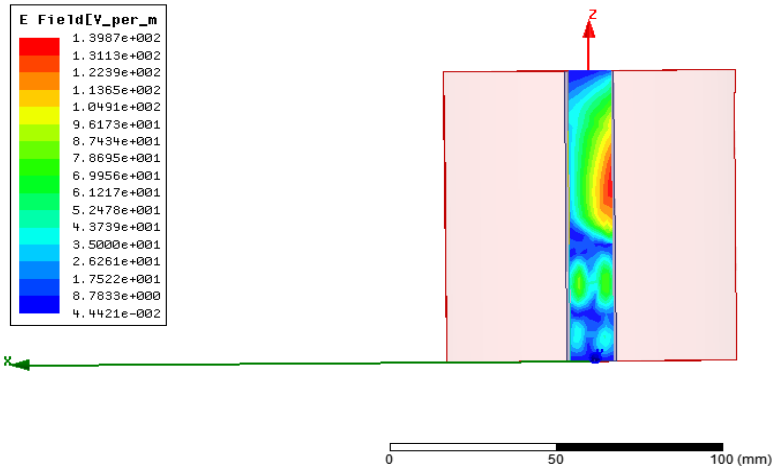

Figure 21: Vertical electrical field distribution cross-section inside sample for 60 ^{o}C of 40% water, 40% oil and 20% gas three phase.

6. CONCLUSIONS

The conclusions can be summarized as follows:

(a) For single-phase experiments, the effect of temperature causes:

(1) A clear frequency and power decrease of S_{11} in the main peak as temperature increases.

(2) A clear frequency increase and power decrease of S_{11} near the 5 GHz frequency peak as temperature increases.
(3) A clear power increase of S_{11} in the 5.45 GHz frequency peak as temperature increases.

(b) For a three-phase water/oil/gas stepped by a 10% change in water and oil contents only with a fixed 20% gas experimental analysis, the effect of phase content changes with constant temperature.
(1) There is a graduated frequency increase of S_{11} with increased WVF in the main peak.
(2) There is a graduated frequency increase of S_{11} with increased WVF near 5 GHz.
(3) The graduated power increases of S_{11} increases the WVF in the 5.45 GHz frequency peak.

The effect of temperature rise at constant phase content causes:
(1) A graduated frequency decrease of S_{11} with increased temperature in the main peak.
(2) A graduated frequency increase of S_{11} with increased temperature near 5 GHz.
(3) A graduated power increase of S_{11} with increased temperature near 5.45 GHz.

(c) The simulation analysis assists the experimental results of the three shifts in frequency or power.
(d) The S_{11} finite element method solution (FEMS) used in simulation is less complicated and shows a decrease in passing EF with an increase in temperature.
(e) This study introduces S_{11} real time monitoring between 3.5-6 GHz frequency as a standardized method to specify the water/oil/gas phase content from the comparison with the studied three peak values and profiles.
(f) The temperature can be specified from the S_{11} values of one of the real-time reading peaks. It then drops it on the standard S_{11} of that phase content. The other two peak readings are used to confirm the temperature specifications.
(g) The measuring method used here has a low power consumption within 0 dB (1.0 mW). This is applicable for safety requirements.

7. ACKNOWLEDGEMENT

The author is grateful to Radio Frequency & Microwave Group at the Faculty of Technology and Environment, Liverpool John Moores University, Liverpool, UK as well as the Dean of the Faculty, Research Assistants and staff for their assistance and access to the laboratory facilities.

8. REFERENCES

[1] Anton Gryzlov, Erik Undheim, Ebbe Nyfors, Lyndall Jordan, Stine Jager Alvaer, and Elin Steinsland, "Challenges With Salinity Measurements in Multiphase Flow Metering", 2012, Emerson Process Magement, Roxar Flow Measurement.
[2] Martin Chaplin, "Water Structure and Science", London South Bank University, UK, March, 2014.
[3] Savarimuthu Robinson and Rangaswamy Nakkeeran, "PC based Optical Salinity Sensor for Different Temperatures", Photonic Sensors, 2012, Vol.2, No.2:187-192.
[4] Anton Cryzlov, Erik Undheim, Ebbe Nyfors, Lyndall Jordan, Stine Jaeger Alvaer, and Elin Steinsland, "Challenges with Salinity Measurements in Multiphase Flow Metering", 2012, Emerson Process Management, Roxar Flow Measurement.
[5] R. Lang, Y. Zhou, C. Utku, and D. Le Vine, "Precise Measurement of the Dielectric Constant of Seawater at 1.413 GHz: The Capillary Exit Hole Correction", 2013, IEEE, 978-1-6473-4778-5-13.
[6] Yan Li, Xue Zhao, Xiao-li Li, and Hai-wei Fu, "Stress and Temperature Sensitivity of Photonic Crystals Resonant Cavity", Hindawi Publishing Corporation, The Scientific World Journal, Vol. 2013, Article ID 805470, 11 pages.
[7] Yu. P. Filippov, I.D. Kakorin, and K.S. Panferov, "Influence of Temperature on the Algorithm to Define Salty Water-in-Oil Flow Characteristics", International Journal of Multiphase Flow Journal, Elsevier, Vol 58, Jan 2014, pp 52-56.
[8] A. El Abd, "Inter Comparison of Gamma Ray Scattering and Transmission Techniques for Gas Volume Fraction Measurements in Two Phase Pipe Flow", Nuclear Instruments Methods in Physics Research section A: Accelerators, Spectrometers, Detectors and Associated equipment Journal, Elsevier, Vol 735, 21 Jan 2014, pp 260-266.
[9] Zhao An, Jin Ningde, Zhai Lusheng and Gao Zhongke, "Liquid Hold-up Measurement in Horizontal Oil-Water Two Phase Flow via a Concave Capacitance Sensor", Measurement Journal, Elsevier, Vol 49, March 2014, pp 153-163.
[10] Chao Tan, Wei Dai, Hao Wu, and Feng Dong, " A Conductance Ring Coupled Cone Meter for Oil-Water Two-Phase Flow Measurement", Sensors Journal, IEEE, Vol 14, Issue 4, pp 1244-1252, April 2014.
[11] Sangbok Park, Young-Seek Chung and Changyul Cheon, "Simple Technique for Measurement of Complex Permittivity and Detection of Small Permittivity Change Using Partially Open Cavity", 2014, J Elect. Eng. Technol. Vol. 9, No.1:268-272.
[12] R.K. Challa, D. Kajfez, J.R. Gladden, and A.Z. Elsherbeni, "Permittivity Measurement With A Non-Standard Waveguide by Using TRL Calibration and Fractional Linear Data Fitting", Progress in Electromagnetics Research B, Vol. 2,1-13, 2008.

[13] V. Komarov, S. Wang, J. Tang, "Permittivity and Measurement", Washington State University, Shankar Anuradha, Art No. eme 308 1-20, 2005.
[14] W. J. Ellison, K. Lamkaouchi and J.M. Moreau, "Water: A Dielectric Reference", J. Mol. Liq. 68(1996) 171-279.
[15] X. Hu, H.A. Buckmaster and O. Barajas, "The 9.355 GHz Complex Permittivity of Light and Heavy Water from 1 ^{o}C to 90 ^{o}C", J. Chem. Eng., Data 39(1994) 625-635.
[16] Lech Rusiniak, "Electric Properties of Water New Experimental Data in the 5 Hz-13 MHz Frequency Range", Institute Geophysics, Polish Academy of Science, Acta Geophysica Polonica, Vol. 52, No.1, 2004.
[17] T. Meissner and F.T. Wentz, "The Complex Dielectric Constant of Pure and Sea Water from Microwave Satellite Observations", IEEE Trans. Geosci. Remote Sensing 42(2004)1836-1849.
[18] Dielectric Constants of Various Materials, Clipper Controls Inc., 2014.
[19] Falcon G., Hewitt G.F., Alimonti C., "Multiphase Flow Metering", Development in Petroleum Science Elsevier, Vol.45, ISSN: 0376-7361, 2009.
[20] Yeung H., "Multi-phase Flow Measurement", Flow Measurement and Instrumentation, Elsevier, 2003.
[21] Pozar, David M. (2005); Microwave Engineering, Third Edition (Intl. Ed.); John Whiley & Sons, Inc.: pp. 170-186, ISBN 0-471-44878-8.